

Optical Engineering

SPIDigitalLibrary.org/oe

Statistical analysis of Airborne Aero-Optical Laboratory optical wavefront measurements

Terry J. Brennan
Donald J. Wittich, III

Statistical analysis of Airborne Aero-Optical Laboratory optical wavefront measurements

Terry J. Brennan

The Optical Sciences Company
Anaheim, California 92806
E-mail: tbrennan@tosc.com

Donald J. Wittich, III

Air Force Research Laboratory
Kirtland AFB, New Mexico 87115

Abstract. The Airborne Aero-Optical Laboratory has produced a large database of aero-optical measurements with a high-speed, high-resolution Shack Hartmann wavefront sensor. The data have been collected over a wide range of flight conditions. An analysis of the statistical characteristics of the subsonic and early transonic data is performed to assess the adequacy of the spatial and temporal resolution of the data. Sample rate requirements for a minimum variance phase estimator are also explored. The techniques employed are validated by application to measurements of optical atmospheric turbulence where results can be anticipated based on established Kolmogorov statistics. © The Authors. Published by SPIE under a Creative Commons Attribution 3.0 Unported License. Distribution or reproduction of this work in whole or in part requires full attribution of the original publication, including its DOI. [DOI: [10.1117/1.OE.52.7.071416](https://doi.org/10.1117/1.OE.52.7.071416)]

Subject terms: Airborne Aero-Optical Laboratory; aero-optic flow; optical phase estimation; optical turbulence; adaptive optics.

Paper 121515SS received Oct. 16, 2012; revised manuscript received Feb. 9, 2013; accepted for publication Feb. 12, 2013; published online Mar. 7, 2013.

1 Introduction and Overview

There is a great deal of interest in understanding the optical degradation due to the aero-optic flow across a turret, or other surface, mounted on an aircraft. It is recognized that the temporal and spatial frequency content of this disturbance may be such that the implementation of conventional techniques of adaptive optics may not be feasible. Consequently, there is interest in the study of active flow control, turret window design, and predictive control schemes for the mitigation of these effects. Predictive control schemes are being studied to address, and perhaps reduce, the high frame rate requirements that are expected.¹

Realistic data are required in order to make advances in this field. Short of simulations based on computational fluid dynamics (CFD), reliable analytic predictions are not available, and CFD simulations are always in need of validation. A major data collection effort, the Airborne Aero-Optic Laboratory (AAOL), has played a significant role in meeting the need for this data. AAOL is an experimental program with the goal of taking direct measurements of the aero-optic disturbance around a turret on an aircraft in flight. Data are collected over a range of flight conditions and turret-pointing angles. The experiment includes two aircraft, a source or beacon aircraft and a receiver aircraft. Flying in formation separated by 50 m ensures that the measured disturbance between the aircraft is due to aero-optical flow and not contaminated by freestream atmospheric turbulence. The receiving turret is 30 cm in diameter with a 10-cm telescope aperture and either a flat or conformal window. A more detailed description of the aircraft and flight conditions can be found in Ref. 2.

This study addresses the nature of the spatial and temporal statistics of the AAOL data. In particular, the questions of adequate temporal and spatial sampling by the AAOL sensor are addressed. Phase and noise-structure functions, described in Sec. 3, are the principal tools

used here. The phase-structure function has been important in the study of atmospheric turbulence, in part because it has a known form that can be identified in measured data.³ Others have looked for similarities in the nature of the aero-optic and free atmospheric turbulence disturbances and have concluded that they are quite different.⁴ In Secs. 3.3 and 3.4 the small separation asymptote of the structure functions of both free-space turbulence and aero-optic turbulence is explored. For atmospheric turbulence it is known that the asymptote is a 5/3-power law³ and Sec. 3.3 will present data to validate this. The aero-optic small separation asymptote also appears to be a power law, but with unity power. It is shown that this conclusion cannot be made with confidence because the temporal sample rate of the AAOL data, although very high, is insufficient to capture the important small separation statistics. The presented measured atmospheric turbulence data is taken from the SOR turbulence sensor (SORTS), an instrument at the Air Force Research Laboratory Starfire Optical Range (SOR). These data are shown because they reveal the importance and effectiveness of handling the measurement error in order to properly estimate the structure function. They also provide a good example of how the structure function from a Shack Hartmann sensor reveals information regarding sample rates.

The required sample rate for data analysis is generally higher than the requirement for control or compensation. Using minimum variance estimation as a predictive tool, a range of control sample rate requirements are developed. This analysis is presented in Sec. 4. A brief discussion on the subject of data quality is presented in Sec. 5. Checking and maintaining data integrity when the data are coming in at a terabyte per test is a challenging, but necessary, task.

This is a purely statistical study. No attempt is made to identify any of the physical processes that produce the measurements or verification of scaling laws. Analysis of that sort can be found elsewhere.⁵⁻⁹

2 AAOL Data

AAOL data used for this study are from the full aperture Shack-Hartmann wavefront sensor, which has 32 subapertures across a 10-cm aperture. Each subaperture is 3.2 mm in the pupil plane of the receiver. The source is a green laser with a wavelength 532 nm. The full subaperture optical path difference (OPD) range is ± 2.2 waves. There are 15 pixels across a subaperture with about 3.4 pixels per λ/d , the diffraction spot size of a subaperture.

The sensor frame rate is generally 20,000 or 25,000 frames per second (fps) for fixed aircraft configuration (both aircraft at the same velocity) and 10,000 to 15,000 frames are collected for each test. For a slewing configuration, where the velocity of the two aircraft is not the same, the frame rate is dropped to 3,000 fps and 40,000 to 45,000 frames are collected. This analysis only considers the fixed configuration and data taken at Mach numbers of 0.5 to 0.61. Data used were taken in February, May, and August of 2011. Although there are two window types used, a flat and a conformal window, this analysis only examines the flat window data.

Raw camera data are saved by the AAOL team and made available for this analysis. Procedures were developed for identifying the aperture location on the camera and the active (illuminated) subapertures, made necessary because the image of the pupil on the camera appears to depend on turret gimbal angles and a new subaperture mask is required for each geometry. The subaperture slope data is calculated with a thresholded centroid on each subaperture. This analysis is independent of that conducted by the AAOL team, and all slope data shown here were processed from raw camera images, with the reconstructed phase produced with a least-squares linear reconstructor, as described in Sec. 3.1.

3 Temporal Structure Functions

The temporal structure function of a random quantity is often useful in understanding the behavior of the quantity over very short and very long time horizons, i.e., the temporal asymptotes. For example, Fried showed³ that the structure function of the optical phase produced by Kolmogorov turbulence is proportional to the 5/3 power of the time separation for small-time separation and the proportionality constant is related to the Greenwood frequency. There is insufficient theory available to characterize the aero-optic structure functions to this level, but computing the sampled structure function of any quantity is generally beneficial.

For the statistical analysis that follows, $\mathbf{x}[k]$ will denote a column vector of real quantities sampled at a discrete time, k . Generally, N_x will denote the number of components of the vector \mathbf{x} and

$$|\mathbf{x}|^2 = \sum_{n=1}^{N_x} x_n^2 \quad (1)$$

defines the norm, $|\mathbf{x}|$, of the quantity. The right hand side of Eq. (1) can also be expressed as

$$|\mathbf{x}|^2 = \mathbf{x}^T \mathbf{x} = \text{trace}(\mathbf{x}\mathbf{x}^T). \quad (2)$$

In the remainder of this analysis the quantity \mathbf{x} is typically going to be values sampled on a grid across the telescope receiver and organized as a column vector. This could be

samples of the optical phase values on a regular grid or Hartmann sensor subaperture slope measurements. If, for example, \mathbf{x} is the discrete phase with the mean removed, then $\sigma_x^2 = |\mathbf{x}|^2/N_x$ would be called the mean-squared phase over the aperture for that frame and the expected value over the ensemble of frames would be the variance of the phase over the aperture.

The temporal structure function will be defined as

$$\mathcal{S}_x^2[n] = \langle |\mathbf{x}[k+n] - \mathbf{x}[k]|^2/N_x \rangle, \quad (3)$$

where the angle bracket, $\langle \cdot \rangle$, denotes the ensemble average over all the statistics. Of course, for sampled data, the average is simply taken over the sample statistics. The form of Eq. (3) reveals certain assumptions about the statistical data. Since $\mathcal{S}_x^2[n]$ does not depend on k it is clear that the data are assumed to be stationary in time. This assumption can be tested and will be discussed in Sec. 4.

Expanding Eq. (3) and assuming stationarity results in

$$\mathcal{S}_x^2[n] = 2\langle |\mathbf{x}[k]|^2/N_x \rangle - 2\langle \text{trace}(\mathbf{x}[k+n]\mathbf{x}[k]^T)/N_x \rangle \quad (4)$$

$$= 2\sigma_x^2 - 2\langle \text{trace}(\mathbf{x}[k+n]\mathbf{x}[k]^T)/N_x \rangle, \quad (5)$$

where the second equality assumes that \mathbf{x} is zero-mean. It is also assumed that for a large-time separation the process is uncorrelated, i.e.,

$$\langle \text{trace}(\mathbf{x}[k+n]\mathbf{x}[k]^T) \rangle = 0, \quad \text{for } n \gg 1. \quad (6)$$

Consequently,

$$\mathcal{S}_x^2[n] = 2\sigma_x^2, \quad \text{for large } n. \quad (7)$$

It is natural to normalize the structure function by the large-time separation asymptote

$$\mathcal{S}_x^2[n]/\mathcal{S}_x^2[\infty] = 1 - \langle \text{trace}(\mathbf{x}[k+n]\mathbf{x}[k]^T)/N_x \rangle/\sigma_x^2, \quad (8)$$

which expresses the relative difference between the temporal covariance and the variance as a function of time separation, n , and goes from zero at $n = 0$ to unity at $n = \infty$.

3.1 Phase-Structure Function

The phase-structure function must be computed from the reconstructed phase. This process, and a simple analysis of measurement error of the reconstruction process, is described in the following paragraphs.

A standard model of the Fried geometry¹⁰ for the Hartmann sensor is used to define a matrix Γ that serves to produce Hartmann slopes, \mathbf{s} , from phase, ϕ , at the corners of the Hartmann subapertures,

$$\mathbf{s} = \Gamma\phi. \quad (9)$$

Sometimes Γ is called a poke matrix, as it can be developed by poking one phase point at a time and recording the response in the sensor. A standard least squares reconstructor is produced from the poke matrix by taking the pseudo inverse

$$H = \Gamma^\dagger. \quad (10)$$

From a measured set of slopes the estimated phase is computed as

$$\hat{\phi} = Hs. \quad (11)$$

The measurements as sensed by the Hartmann sensor can be represented as

$$s = \Gamma\phi + \mu, \quad (12)$$

where μ can be taken to be a general measurement error with zero mean. It includes the error due to sensor noise, as well as the modeling error inherent in Γ . It will be assumed that μ is uncorrelated between subapertures, that is,

$$\langle \mu\mu^T \rangle = \sigma_\mu^2 I, \quad (13)$$

where I is the identity matrix and σ_μ^2 is the variance of each component of the measurement error. Combining Eqs. (11) and (12) results in

$$\hat{\phi} = H\Gamma\phi + H\mu. \quad (14)$$

The measurement error propagates into the reconstructed phase as $H\mu$ whose variance can be calculating using Eq. (13),

$$\begin{aligned} \text{trace}(\langle H\mu\mu^T H^T \rangle) / N_{\hat{\phi}} &= \text{trace}(H\langle \mu\mu^T \rangle H^T) / N_{\hat{\phi}} \\ &= \sigma_\mu^2 \text{trace}(HH^T) / N_{\hat{\phi}}. \end{aligned} \quad (15)$$

Consequently the noise gain associated with the reconstructor H will be denoted

$$\beta_H = \text{trace}(HH^T) / N_{\hat{\phi}}. \quad (16)$$

Equation (14) reveals that the structure function of the reconstructed phase should be related to the structure function of the phase and the structure function of the measurement error. This will clearly be true if phase and measurement error are assumed to be independent, i.e., $\langle \phi[H\mu]^T \rangle = 0$. In addition, the quantity $H\Gamma$ is essentially the identity matrix. In fact, it is known that the only two modes that are not observed by a Hartmann sensor are piston and waffle. So $\phi = H\Gamma\phi$ up to piston and waffle. Thus the structure function of ϕ is essentially given by

$$\mathcal{S}_{\hat{\phi}}^2(\tau) = \mathcal{S}_{\phi}^2(\tau) - \mathcal{S}_{H\mu}^2(\tau) = \mathcal{S}_{\phi}^2(\tau) - \beta_H \mathcal{S}_{\mu}^2(\tau) \quad (17)$$

and it remains to determine the measurement error propagation structure function, $\mathcal{S}_{\mu}^2(\tau)$. Note that these expressions use continuous-time notation with arguments in parentheses, (τ) , and discrete time was expressed in Sec. 3 with arguments in brackets, $[n]$.

3.2 Noise-Structure Function

The variance of the measurement error, or “noise,” can be estimated directly from the wavefront sensor measurement, s . First, project the reconstructed phase back into sensor space using Eq. (14) and a property of the pseudo-inverse, $\Gamma H\Gamma = \Gamma$,

$$\begin{aligned} \hat{s} &= \Gamma\hat{\phi} = \Gamma(H\Gamma\phi + H\mu) \\ &= \Gamma\phi + \Gamma H\mu. \end{aligned} \quad (18)$$

Subtracting the reconstructed measurement from the actual measurement using Eq. (12)

$$\delta = s - \hat{s} = \mu - \Gamma H\mu = (I_s - \Gamma H)\mu. \quad (19)$$

Here I_s is the identity on sensor measurements. The quantity δ is often called the slope discrepancy. It is that part of the measurement that is not reconstructed by a least-squares reconstructor. The slope discrepancy operator is

$$\mathcal{D} = (I_s - \Gamma H). \quad (20)$$

From the properties of the pseudo-inverse and Eq. (12) it is easy to see that \mathcal{D} is a projection operator with the following properties

$$\mathcal{D}\mathcal{D} = \mathcal{D}, \quad (21)$$

$$\mathcal{D}\Gamma = 0, \quad (22)$$

$$\mathcal{D}s = \mathcal{D}\mu. \quad (23)$$

Again assuming that μ is spatially white [Eq. (13)], the variance of δ is

$$\begin{aligned} \sigma_\delta^2 &= \text{trace}(\langle \mathcal{D}\mu\mu^T \mathcal{D}^T \rangle) / N_s \\ &= \sigma_\mu^2 \text{trace}(\mathcal{D}\mathcal{D}^T) / N_s. \end{aligned} \quad (24)$$

Since \mathcal{D} is a projection operator $\text{trace}(\mathcal{D}\mathcal{D}^T)$ is equal to $\text{trace}(\mathcal{D})$. From Eq. (22) the null space of \mathcal{D} is the range space of Γ . The range space is of rank $N_s - 2$ where the 2 reflects the fact that piston and waffle are in the null space of Γ . So

$$\text{trace}(\mathcal{D}) = N_s - \text{trace}(\Gamma) = N_s - N_\phi + 2. \quad (25)$$

Using this and Eq. (24) the variance of the measurement error can be calculated

$$\sigma_\mu^2 = \frac{N_s}{N_s - N_\phi + 2} \sigma_\delta^2. \quad (26)$$

The fraction in this expression is simply the ratio of vector space dimensions. The numerator is the dimension of the measurement space and the denominator is the dimension of the slope discrepancy subspace and the ratio is the scaling up of the slope discrepancy variance to measurement (or slope) space. This ratio will be denoted

$$\beta_{\mathcal{D}} = \frac{N_s}{N_s - N_\phi + 2}. \quad (27)$$

Equation (26) says that if the measurement is white noise with unity variance then the slope discrepancy variance is $1/\beta_{\mathcal{D}}$.

The variance scaling expressed in Eq. (26) obviously holds for the structure function as well

$$\mathcal{S}_{\mu}^2(\tau) = \beta_{\mathcal{D}} \mathcal{S}_{\delta}^2(\tau). \quad (28)$$

Substituting Eq. (28) into Eq. (17)

$$\mathcal{S}_\phi^2(\tau) = \mathcal{S}_\phi^2(\tau) - \beta_H \beta_D \mathcal{S}_\delta^2(\tau). \quad (29)$$

Thus the noise corrected phase-structure function can be calculated from the reconstructed phase-structure function and the properly scaled slope discrepancy structure function.

3.3 Atmospheric Turbulence

Before applying the structure function analysis approach to AAOL data, the validity of the approach will be demonstrated using data collected over horizontal propagation paths, where the disturbance is purely atmospheric turbulence. A solid theory in weak turbulence is available from which comparisons with measurement data can be performed. The phase-structure function can be calculated under the assumption of Kolmogorov turbulence and the short time separation asymptote is known to be³

$$\lim_{\tau \rightarrow 0} \mathcal{S}_\phi^2(\tau) = 28.4(f_G \tau)^{5/3}, \quad (30)$$

where f_G is the Greenwood frequency. If the structure function is calculated from measurement data and reveals the 5/3-power law, then Eq. (30) can be used to estimate the Greenwood frequency. The presence of the 5/3-power law also indicates the validity of the assumption of Kolmogorov turbulence. A great deal of data has been taken with an instrument at the Starfire Optical Range (SOR), which is called the SOR turbulence sensor (SORTS). A publication on this instrument and the data collected will be available in the near future. The instrument is a 32×32 Shack Hartmann wavefront sensor in a Meade 40 cm telescope. It is typically used with a HeNe laser as a point source and has about ± 3 waves of linear range per subaperture and 18 pixels across each subaperture. It is not unlike the AAOL wavefront sensor, except for a much larger aperture and a telescope without struts. The absence of the struts

improves the quality of the collected data in several ways. Most obviously the absence of struts increases the percentage of unobscured subapertures, but it is also advantageous to compute various slope-related quantities, such as the slope discrepancy, on a connected region.

Figure 1 shows two examples of the application of Eq. (29) to data collected with SORTS. Figure 1(a) was taken over a 50-m path in weak turbulence. For this case the Fried coherence length, r_0 , is 15.6 cm and the Greenwood frequency is 6.9 Hz. In Fig. 1(b) the structure function estimate is shown for strong turbulence over a 3200-m path resulting in $r_0 = 1.0$ cm and $f_G = 121$ Hz. Both figures are plotted on the same scale in units of waves.² Each of the three structure functions are shown in the figures. The reconstructed phase is the dashed curve. The estimated noise (or measurement error) structure function is the dash-dot curve and the difference is the solid curve. The difference, labeled noise-removed structure function, shows a strong small τ asymptote of $\tau^{5/3}$. The dotted curve is a 5/3-power law plotted for reference. These data are among the best collected by SORTS, in terms of agreement with theory, but they are not atypical. The 5/3-power law is almost always present, but does not always persist over as many decades as seen in these data. The theory underlying this analysis assumes weak turbulence, but its application to the very strong case in Fig. 1(b), where the Rytov number is estimated to be about two, continues to produce valid and interesting results.

3.4 AAOL Structure Functions

Having demonstrated the value of examining phase-structure functions for atmospheric turbulence, the AAOL data will now be considered. Data from flight campaigns conducted in February, May, and August 2011 have been studied. The data in February and May were taken in the subsonic regime at a Mach number of 0.5. The August data approach the transonic regime with Mach numbers between 0.6 and 0.65. According to Ref. 11, the turret is expected to have a

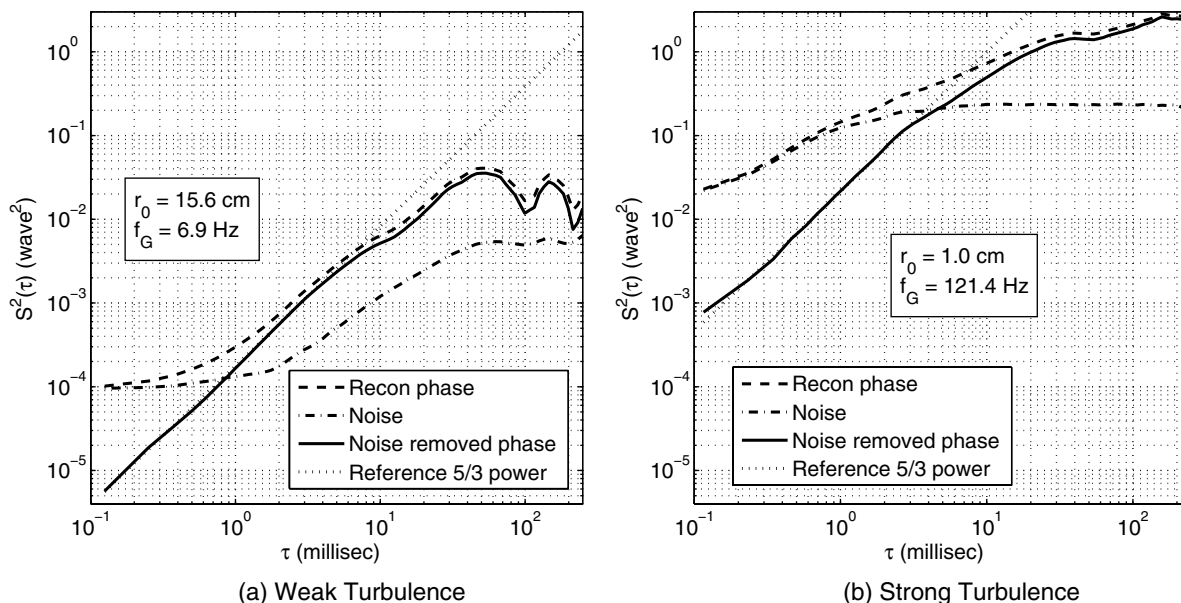


Fig. 1 Phase structure function for atmospheric turbulence.

freestream critical Mach number around 0.55, above which portions of the local air flow (i.e., near the turret) exceed the speed of sound. Analysis of the optical data for the conformal window turret at Mach 0.6 showed the presence of a shock on the window when viewing through the region of minimum pressure,⁵ indicating transonic flow.

Figure 2 shows representative data for Mach 0.5 and 0.61. These were taken with a flat window. A range of lines of sight (LOS) or viewing angles between 98 deg and 115 deg are shown. The LOS is the composite angle between the turret pointing angle and the reverse flow direction. This angle has been defined and shown to be useful by other researchers as a single parameter for characterizing features of the optical flow.^{2,5,7,8,11} It is given by

$$\cos(\text{LOS}) = \cos(\text{Azimuth Angle}) \cos(\text{Elevation Angle}). \tag{31}$$

The features of the data in Fig. 2 are clearly different than what has been observed for the case of atmospheric turbulence in Fig. 1. The noise, or measurement error, structure functions are well below the phase-structure function. Consequently the noise-corrected structure function (difference of phase and noise) has not been displayed as it was for the atmospheric turbulence data. Looking at the phase-structure functions a number of conclusions can be drawn. At small time separation the phase-structure function has not yet reached a noise floor and looks more like a unity power law than the atmospheric $\tau^{5/3}$. A plot of τ^1 is shown as a dotted curve for reference. For the atmospheric data the small separation noise floor was clearly seen especially for the weak turbulence case. The existence of this floor implies that the sampling is sufficiently fast that the difference of two adjacent frames of data is dominated by noise, i.e., the disturbance has not changed in one frame so it is subtracted out. This cannot be concluded for the AAOL data. In no case were the data observed to reach the noise floor in the February, May and August data of 2011. Recalling that the

large separation asymptote is twice the variance from Eq. (7), these figures show a large range of variances. In terms of the relative covariance error which according to Eq. (8) is the ratio of the structure function to the large separation asymptote these data show values of between 1/5 to 1/3.

It can be concluded that the AAOL measurements do not capture all of the highest temporal frequencies at the current frame rate. The May data (Mach 0.5) were taken at 20 kilo frames per second (kfps) and the August data were taken at 25 kfps. There would be value in going to higher frame rates. For reference, the atmospheric data taken with SORTS were collected at 8 kfps. A simple extrapolation of the phase-structure functions in Fig. 2 imply that frame rates of five to six times higher than the AAOL frame rate would be required to reach the noise floor. This would be 100 to 125 kfps.

The phase-structure functions all tend to flatten out for time separations greater than one millisecond. This implies that the phase is uncorrelated over time differences greater than a millisecond. Consequently, the sample rate for any adaptive optics system, even using advanced predictive techniques, must be greater than 1000 fps.

Looking at the noise-structure function leads to additional insights. These are basically flat or just barely beginning to attenuate at the smallest time separations. As was described in Sec. 3.2 the term noise is used in a general sense and using the term measurement error might be more appropriate. The noise-structure functions in Fig. 1 due to atmospheric turbulence show two plateaus. The small separation plateau is due to temporally uncorrelated noise. The turbulence has not changed between two consecutive frames relative to the pure noise level. As τ , the time separation, increases the noise-structure function transitions to the next plateau. The turbulence contribution in the frame differences grows with separation and couples into measurement error. The second plateau is reached and maintained at the time separation when the turbulence is uncorrelated with its level depending on the subaperture size. It will be higher for larger subapertures, since higher frequency phases will not be sensed well

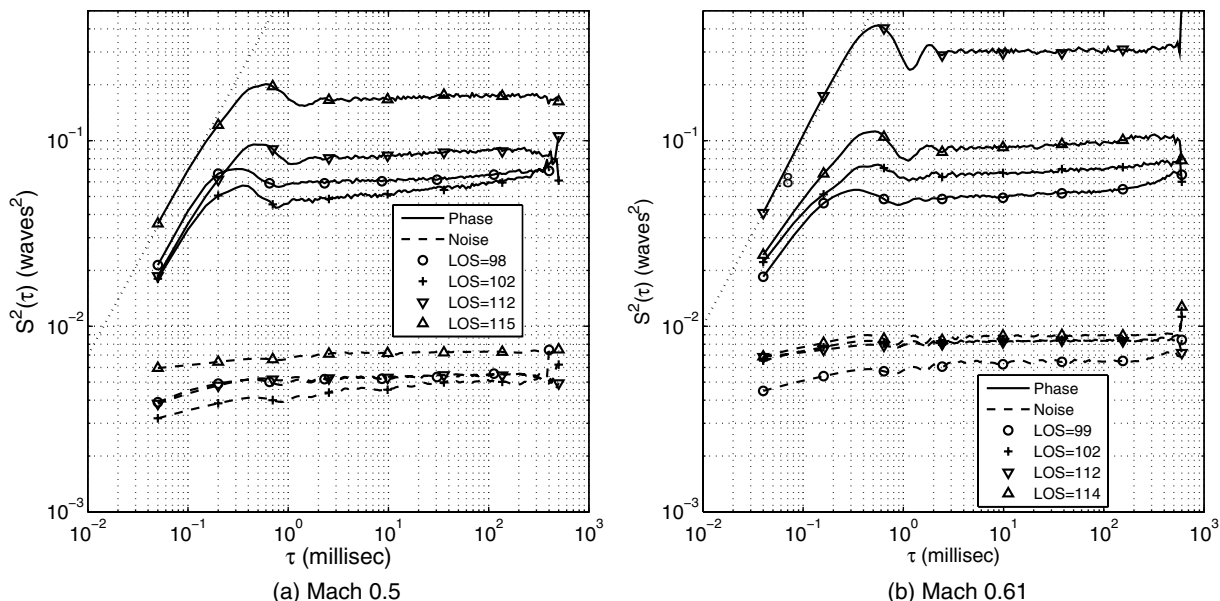


Fig. 2 Aero-optic phase structure functions.

as the resolution of the sensor decreases. In fact, for Kolmogorov turbulence it will grow as $d^{5/3}$, where d is the width of the subaperture. This is very clear for the weak turbulence case in Fig. 1. The strong turbulence case has a high Greenwood frequency and the small separation plateau is not fully reached at the sample rate of the data. In the atmospheric data the transition to the upper plateau occurs at about the same place that the phase-structure function begins to level off. Compared to the atmospheric data, the aero-optic noise-structure function is very flat with little fall-off as the phase falls off. This, plus the observation that the noise does not vary from case to case as much as the phase varies, suggests that the noise is essentially just ordinary signal noise with little coupling of disturbance into the measurement error. From this it can be concluded that the spatial resolution of the sensor is more than sufficient to accurately measure these disturbances. In fact, a future design could consider fewer subapertures in order to achieve higher temporal frame rates.

In developing predictive control schemes the repeatability of propagation statistics, given the same defining parameters, is assumed and the sensitivity to small changes in defining parameters is expected to be small. Predictive control schemes may be based on developing a library of control gains that can be scheduled according to a small set of parameters. These parameters would certainly include Mach number and turret pointing angle, but may require other parameters, as well. Such a library would be, of necessity, based on discrete values of the parameters and the scheduled gains should perform well over small tolerances around the discrete values. Some approaches are adaptive and have the capability to slowly update their gains as conditions change. In either case, it is reasonable to hope that no change in parameters would result in no change in statistics, given that the right set of parameters are known and small changes in parameters would produce small changes in statistics. To the author's knowledge, no comprehensive study has considered this issue although there have been suggestions that AAOL repeat some of the flight conditions from previous campaigns and compare the results with earlier data.

Upon searching the available data two cases were discovered that had been collected under nearly identical conditions. They were both collected at Mach 0.5, with a LOS of 98 deg and very similar azimuth and elevation angles. Their structure functions are shown in Fig. 3. One of them has a phase-structure function that is 18% higher than the other and a noise-structure function that is 41% higher than the other. This difference could be the result of something as innocuous as an error in recording the parameters but it may suggest a level of sensitivity of the disturbance to small changes in the geometric parameters. There are factors in the equipment that could produce different measurement statistics, such as an optical alignment difference or a defocus in the lenslet array. However, these cases were run consecutively as if the source laser were turned on, then off, then on, and then off without any change in flight conditions of the two aircraft. Repeatability is hard to test on the SORTS sensor because nature always gives us a different turbulence distribution (C_n^2) along the path. Even if two turbulence cases give the same r_0 they might differ significantly in other parameters. The aero-data should only

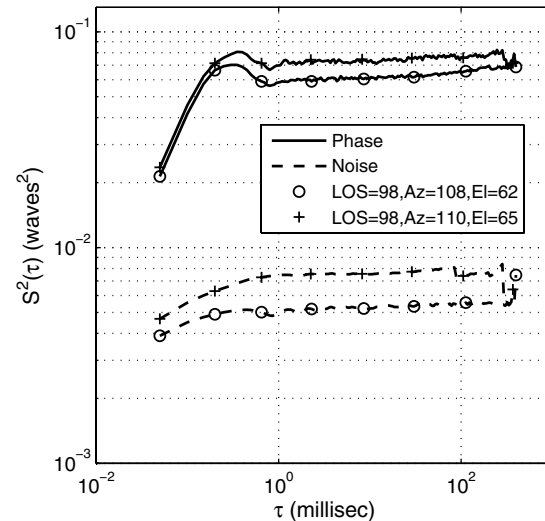


Fig. 3 Aero-optic structure functions for two, nearly identical, geometries at Mach 0.5.

depend on Mach number, turret geometry and pointing angles.

Gordeyev et al.¹² showed that, for a two-dimensional (2-D) turret in a confined tunnel, a sharp change in the higher-order aero-optics occurred around LOS = 98 deg as the flow transitions from partially to fully separated. Porter et al.⁸ showed that, for a three dimensional (3-D) turret, the same phenomenon depended on both elevation and azimuth, even for the same LOS. However, Porter's analysis also suggested that the fluid dynamics should not be terribly sensitive at these particular combinations of azimuth and elevation, which are viewing fully separated flow, but in the region where higher-order OPD is declining due to aperture effects. The small changes in angle could certainly account for some of the changes in the statistics, but the authors cannot offer a full explanation for the discrepancy at this time.

4 Wavefront Estimation

The temporal structure function naturally contains information about wavefront estimation. If $\phi[k]$ is a sequence of wavefront phases across an aperture then $S_\phi^2[m]$ is the mean-squared error that would be experienced if the current frame of data is estimated by the frame of data that is m frames prior. In particular $S_\phi^2[1]$ is the mean-squared error when the current frame is estimated by the previous frame. Note that this discussion is using discrete time and the real time depends on the sample rate. The estimation error represented by $S_\phi^2[m]$ will be called m frame hold. Only one frame hold will be presented in this analysis but variable frame rate will be considered.

Since the wavefront data were taken at a very high rate, either 20 kfps or 25 kfps, it can be subsampled at different levels to simulate the estimation performance at different frame rates. For example, the subsampled set $\{\phi[k]: k = 1:m:N_\phi\}$ simulates frame rates of 20, 10, 6.67, and 5 kfps when ϕ is sampled at 20 kfps and $m = 1, 2, 3,$ and 4.

A more optimal estimator than 1-frame hold will also be considered. This will be a standard minimum variance estimator which uses the matrix gain A that minimizes

$$\begin{aligned}
 J &= \langle |\phi_{k+1} - A\phi_k|^2 \rangle \\
 &= \text{trace}(\langle (\phi_{k+1} - A\phi_k)(\phi_{k+1} - A\phi_k)^T \rangle) \\
 &= \text{trace}(\langle \phi_{k+1}\phi_{k+1}^T \rangle - 2\langle \phi_{k+1}\phi_k^T \rangle A^T + A\langle \phi_k\phi_k^T \rangle A^T).
 \end{aligned}
 \tag{32}$$

The notation

$$C_{m,n} = \langle \phi_m\phi_n^T \rangle \tag{33}$$

will be used for the covariance matrices. Note that $C_{k+1,k+1} = C_{k,k}$ since stationarity is assumed. With this notation J is expressed more simply as

$$J = \text{trace}(C_{k,k} - 2C_{k+1,k}A^T + AC_{k,k}A^T). \tag{34}$$

Taking the partial derivative of J with respect to A produces

$$\frac{\partial J}{\partial A} = -2C_{k+1,k} + 2AC_{k,k}. \tag{35}$$

Setting this to zero and solving for A produces the minimum variance gains

$$A = C_{k+1,k}C_{k,k}^{-1}. \tag{36}$$

To apply this estimation process, a sequence of AAOL reconstructed phases will be tilt and piston removed and then used to numerically compute the sample covariances $C_{k,k}$ and $C_{k+1,k}$. Three estimation techniques will be evaluated with the following error expressions:

$$\text{1-frame hold: } \frac{1}{N-1} \sum_1^{N-1} (\phi_{k+1} - \phi_k)^2$$

$$\text{optimal: } \frac{1}{N-1} \sum_1^{N-1} (\phi_{k+1} - A\phi_k)^2$$

$$\text{split data optimal: } \frac{1}{N/2-1} \sum_{N/2+1}^{N-1} (\phi_{k+1} - A_s\phi_k)^2.$$

The ‘‘split data’’ version of the minimum variance estimate is a more realistic evaluation of the optimal estimation error. In this version the covariance matrices and optimal gain, A_s , are calculated from the first half of the measurement sequence and evaluated on the second half. This is a method of handling the problem of a sample data covariance operating on the same data that were used in its calculation and achieving unrealistically favorable results. With finite sample sizes this type of independent evaluation of performance is necessary. If the optimal and split data optimal performance are close then the data are reasonably stationary and there are likely sufficient samples in the calculated covariance.

The estimation performance will be plotted for a collection of Mach 0.5 AAOL data taken in 2011. It will be plotted as a function of the view angle, LOS. The interest here is in comparative errors, so rather than plot the mean-squared error a simulated Strehl ratio will be calculated via the Marechal approximation

$$S = \exp(-\sigma_E^2), \tag{37}$$

where E is the residual phase estimation error in radians. All the data that will be considered were collected at 20 kfps so performance will be evaluated at 20, 10, and 5 kfps by decimating as described above.

Another simplification will be made to expedite the calculations. The phase vectors are typically over 700

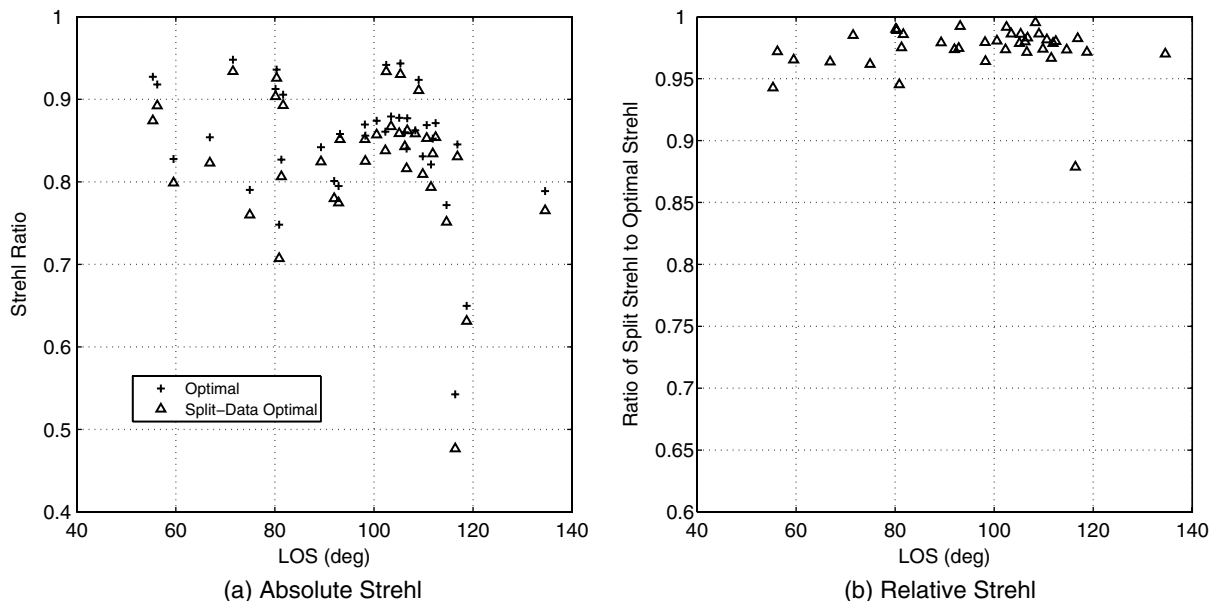


Fig. 4 Comparison of full optimal with split-data optimal.

components long. Analysis of the data shows that over 98% of the power is contained in the first 200 Karhunen Loeve modes. So the coefficients of this 200 dimensional modal subspace will be used rather than the roughly 730 dimensional phase space. (The Karhunen-Loeve decomposition is referred to as the Proper Orthogonal Decomposition by other researchers in this field^{7,13})

The first item to be noted from this analysis of the data is shown in Fig. 4. Here the “Full optimal” and “Split-Data optimal” are shown as a function of LOS for the 20 kfps data. In Fig. 4(a) the Strehl performance is shown and in Fig. 4(b) the ratio of split to optimal Strehl ratio is shown. The data show that the split data performance is greater than 95% of the full optimal performance in almost all cases except for one outlier at a LOS of about 115 deg. This results in a strong conclusion that the data are statistically stationary over the

sequence. That is, the sample statistics of the first half of the sequence is in good agreement with the full sequence. In the remainder of the performance evaluations only the more realistic split-data optimal will be presented.

The estimation performance data are shown as Strehl ratios in Fig. 5(a) for the 20 kfps data. This shows how the general performance degrades with increasing LOS angle. An immediate observation from this data is that the split-data optimal always performs better than the 1-frame lag, except perhaps at forward looking angles where the performance is similar. The 1-frame lag always performs better than open loop.

To better quantify the relative performance and to assess the performance as the frame rate is reduced consider Fig. 5(b) through 5(d). In these figures the Strehl Ratio of the optimal and 1-frame lag estimators is divided by

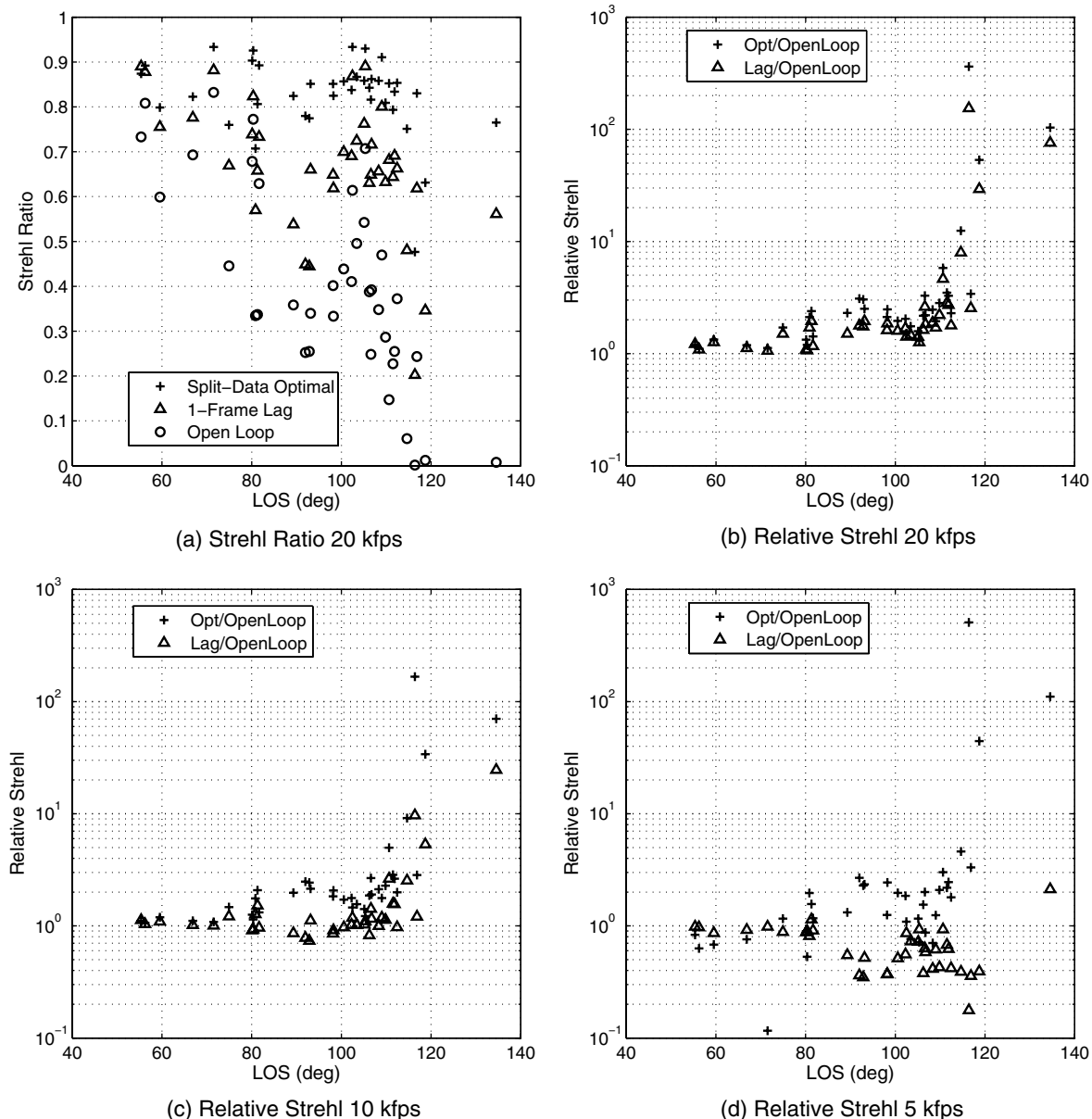


Fig. 5 Comparative Strehl ratio performance.

the open loop Strehl ratio indicating the performance improvement available with predictive methods. The results for a frame rate of 20 kfps are shown in Fig. 5(b). At forward looking angles the performance gains of both optimal and 1-frame lag estimators are about the same. As the LOS angle increases the performance improvements increase and the optimal estimates are clearly better than 1-frame lag estimates. At the lower frame rate of 10 kfps, shown in Fig. 5(c), the optimal estimates perform almost as well as the 20 kfps performance but the 1-frame lag loses performance and for LOS angles between 80 deg and 110 deg the 1-frame lag performance is often worse than open loop. Finally, Fig. 5(d) shows results for 5 kfps where the 1-frame lag almost always performs worse than open loop with performance becoming much worse than open loop for backward looking angles. This implies that a single subaperture measurement is essentially uncorrelated in time at a frame rate of 5 kfps. The optimal estimation continues to perform better than open loop, at least for angles greater than 80 deg. The optimal estimator is able to estimate a subaperture measurement by extracting information from adjacent subaperture measurements even at this slowest rate.

5 Data Integrity

When the available data from an experiment are limited, it is feasible to carefully examine the data and validate their integrity in order to develop a high level of confidence in the results. When the data are measured in multiple terabytes it becomes nearly impossible to look at each data case for anomalous behavior. The tendency is to turn the crank and crunch the data with a batch processing approach. The AAOL has been collecting data for two years and has accumulated a very large, and still growing, database. Over this time the methodology for experiment execution and data collection has certainly matured and important lessons continue to be learned that increase the confidence in the reliability of the results. Nonetheless it remains prudent to spot check the raw, intermediate, and final processed results on a regular basis to minimize the possibility of new, or old, problems creeping into the data.

No data are ever perfect but it is generally possible to quantify the impact of data variations and anomalies on important numerical results. In examining the 2011 data a significant level of saturated pixel data was observed. This was particularly problematic in the February data. Techniques were developed to estimate how this would impact results like the structure functions and Strehl estimates that have been presented here and it was found that the observed level of saturation had an impact of only a few percent. In fact, the two data sets in Fig. 3 both have some level of saturation but not enough to account for the unexpected differences between them. Our analysis of the raw camera data also revealed amplitude scintillation, the cause of which has not yet been determined.

6 Conclusions

The goal of the AAOL program is to understand the nature of aero-optic disturbances over a wide range of conditions and develop techniques to mitigate the optical degradations. To this end the AAOL data have proven to be an extremely valuable asset. Using the tools of structure-function analysis and

optimal estimation, it has been demonstrated that the spatial resolution of the AAOL wavefront sensor is more than adequate for disturbance characterization at least in subsonic and early transonic regimes. The temporal resolution remains challenging and it would be desirable to increase the frame rate of the AAOL sensor by a factor of five or six. This means 100 to 125 kfps. This may be doable with current camera technology by reducing the spatial sampling by a factor of two. Nonetheless the current data were shown to be adequate for studying phase-estimation sampling requirements for development and implementation of predictive control schemes. These results indicate that sample rates for closed loop control can be dropped to as low as 5 kfps when a predictive estimation and control scheme is implemented. Traditional control will fail at any rates less than 10 kfps with only marginal performance at 10 kfps. Of course, as mentioned, these conclusions only apply to subsonic and early transonic data and do not address the issues of slewing turrets. Repeatability and sensitivity to parameters are issues that need continued study as evidenced by the data in Fig. 3.

Acknowledgments

This work was supported by the Air Force Research Laboratory (AFRL) under contract number FA9451-11-C-0140 with the Optical Sciences Company (tOSC). The views and conclusions expressed here are not those of the US Air Force but strictly those of the authors. The authors wish to acknowledge the assistance of the AAOL team at University of Notre Dame and MZA Corporation for their help in obtaining and understanding the AAOL data. We also thank the Starfire Optical Range ASALT team for allowing us to present the turbulence data from SORTS.

References

1. J. Tesch and S. Gibson, "Receding-horizon adaptive control of aero-optical wavefronts," *Proc. SPIE* **8395**, 83950B (2012).
2. E. J. Jumper et al., "The airborne aero-optics laboratory, AAOL," *Proc. SPIE* **8395**, 839507 (2012).
3. D. L. Fried, "Time-delay-induced mean-square error in adaptive optics," *J. Opt. Soc. Am. A* **7**(7), 1224–1225 (1990).
4. J. P. Siegenthaler, E. J. Jumper, and S. Gordeyev, "Atmospheric propagation vs. aero-optics," in *46th AIAA Aerospace Sciences Meeting and Exhibit*, AIAA 2008-1076, AIAA, Reno, Nevada (2008).
5. N. De Lucca, S. Gordeyev, and E. Jumper, "The airborne aero-optics laboratory, recent data," *Proc. SPIE* **8395**, 839508 (2012).
6. S. Gordeyev et al., "Aero-optical environment around a cylindrical turret with a flat window," *AIAA J.* **49**(2), 308–315 (2011).
7. D. J. Goorskey, R. Drye, and M. R. Whiteley, "Spatial and temporal characterization of AAOL flight test data," *Proc. SPIE* **8395**, 839509 (2012).
8. C. Porter et al., "Flight measurements of aero-optical distortions from a flat-windowed turret on the airborne aero-optics laboratory (AAOL)," in *42nd AIAA Plasmadynamics and Lasers Conf.*, AIAA-2011-3280, AIAA, Honolulu, Hawaii (2011).
9. N. De Lucca, S. Gordeyev, and E. Jumper, "Comparison of aero-optical measurements from the flight test of full and hemispherical turrets on the airborne aero-optics laboratory," in *43rd AIAA Plasmadynamics and Lasers Conf.*, AIAA-2012-2985, AIAA, New Orleans, Louisiana (2012).
10. D. L. Fried, "Least-square fitting a wave-front distortion estimate to an array of phase-difference measurements," *J. Opt. Soc. Am.* **67**(3), 370–375 (1977).
11. S. Gordeyev and E. Jumper, "Fluid dynamics and aero-optics of turrets," *Prog. Aerosp. Sci.* **46**(8), 388–400 (2010).
12. S. Gordeyev et al., "The optical environment of a cylindrical turret with a flat window and the impact of passive control devices," in *36th AIAA Plasmadynamics and Lasers Conf.*, AIAA-2005-4657, AIAA, Toronto, Ontario, Canada (2005).
13. S. Abado, S. Gordeyev, and E. J. Jumper, "AAOL wavefront data reduction approaches," *Proc. SPIE* **8395**, 83950A (2012).



Terry J. Brennan received his PhD in mathematics from the University of California Irvine. He has been a senior scientist at the Optical Sciences Company (tOSC) for the past 23 years; prior to that he worked for 10 years at The Aerospace Corporation. He has worked on a wide range of problems associated with adaptive optics systems, including issues of performance, stability, and atmospheric characterization. He is the principal architect of WaveProp, tOSC's wave optics simulation class library.



Donald J. Wittich, III received his PhD in aerospace engineering from the University of Notre Dame in 2010. He joined the Air Force Research Laboratory's Directed Energy Directorate in 2009, where he currently serves as principal investigator for aero-optical and aero-mechanical research. His research interests include aero-optics, fluid dynamics, and flow control.